# Heavy REE are compatible in clinopyroxene on the spinel lherzolite solidus

J.D. Blundy *, J.A.C. Robinson, B.J. Wood

*CETSEI, Department of Earth Sciences, University of Bristol, Wills Memorial Building, Bristol BS8 1RJ, UK*

## Abstract

Trace element partitioning between clinopyroxene and melt was investigated experimentally under conditions appropriate to near-solidus melting of spinel lherzolite in the upper mantle. Starting material was a high-Na, Al basalt glass previously shown to be a very low degree ($\sim$1%) partial melt of spinel lherzolite at 1.5 GPa, 1269ºC [Robinson et al., Earth Planet. Sci. Lett., in press]. The experiment was run with a spinel seed under sub-liquidus conditions (1255ºC) to ensure clinopyroxene crystallisation. The experimental clinopyroxene composition is consistent with equilibrium close to the solidus of fertile mantle lherzolite, most notably in its high contents of Ca-Tschermak's (CaTs) molecule ($\sim$22 mol %) and $Na_2O$ (1.4 wt%). Clinopyroxene–melt partition coefficients ($D$) for a wide range of trace elements, determined by SIMS analysis of run products, differ markedly from those reported in other studies under conditions less appropriate to mantle melting. In particular partition coefficients for the heavy rare earth elements (Gd–Lu) are greater than unity (e.g. $D_{Lu} = 1.45$), and the critical partitioning parameter, $(D_{Sm}/D_{Nd}) \times (D_{Hf}/D_{Lu})$, is 0.68. These features, which arise due to the high CaTs content of the clinopyroxene, dramatically reduce the required involvement of garnet in the melting region beneath mid-ocean ridges. © 1998 Elsevier Science B.V. All rights reserved.

*Keywords:* trace elements; partitioning; mantle; melting; mid-ocean ridge basalts; spinel lherzolite; clinopyroxene; rare earths

## 1. Introduction

There is an emerging consensus that a significant proportion of mantle melting that occurs beneath mid-ocean ridges takes place in the garnet stability field. This conclusion is based upon several independent lines of geochemical evidence from mid-ocean ridge basalts (MORB): (1) the rare earth element (REE) signature of MORB glasses [1] and glass inclusions [2]; (2) REE patterns of clinopyroxenes in abyssal peridotites [3]; (3) Sm–Nd and Lu–Hf isotope systematics [4,5]; and (4) U–Th isotopic disequilibrium [6]. Interpretation of all these features is strongly dependent upon assumptions made about the partitioning behaviour of the relevant trace elements under mantle melting conditions. Critical in this respect are Nernst partition coefficients ($D$ = concentration in crystal/concentration in melt) for clinopyroxene and garnet, which determine the evolution of trace elements during mantle melting. As partition coefficients depend on temperature ($T$), pressure ($P$), composition ($X$), and, in the case of polyvalent cations, oxygen fugacity ($f_{O_2}$) it is essential, when incorporating experimental partition coefficients into geochemical models, that experi-

* Corresponding author. Fax: +44 (117) 925-3385; E-mail: jon.blundy@bris.ac.uk

mental and model $P$–$T$–$X$–$O_2$ conditions be carefully matched. Failure to do this leads to the use of inappropriate partition coefficients and consequent misinterpretation of chemical data. Here we demonstrate that partitioning of trace elements between clinopyroxene and silicate melts under conditions appropriate to partial melting at the spinel lherzolite solidus differs substantially from that previously inferred, leading to a significant diminution of the importance of garnet lherzolite melting in MORB petrogenesis.

## 2. Experimental design and conditions

In the spinel lherzolite field, near-fractional melting of fertile mantle generates melts that are chemically distinct from those produced at higher melt fractions. Low-degree melts are demonstrably richer in $SiO_2$, $Al_2O_3$ and $Na_2O$ [7–9]. Similarly the compositions of residual solid phases differ close to the solidus. Near-solidus clinopyroxene has higher Ca-Tschermak's (CaTs) and jadeite contents than clinopyroxene produced at higher melt fractions [7] and these compositional differences are likely to affect the partitioning behaviour of trace elements. For example, it has been shown [8] that clinopyroxene–melt $D_{Ti}$ close to the spinel lherzolite solidus at 1 GPa is a factor of three higher than at higher melt fractions, while high $D_{REE}$ for CaTs-rich clinopyroxenes have been observed by a variety of workers in synthetic, Fe-free systems [10–12]. Using the partitioning model of Wood and Blundy [13], Blundy and Brodie [14] have shown that the predicted clinopyroxene–melt partition coefficients for heavy rare earth elements (HREE) on the spinel lherzolite solidus are ~50% higher (e.g. $D_{Lu} = 0.85$) than values commonly used in geochemical modelling (e.g. [15]), so that, in terms of HREE partitioning, clinopyroxene resembles garnet ($D_{Lu} = 3.8$ [16]) more closely than previously thought. Such large values of clinopyroxene $D_{HREE}$ lead to buffering of HREE concentrations in mantle melts without any involvement of garnet in the melting region. The Wood and Blundy [13] model was not, however, calibrated on liquids as sodic and aluminous as those on the spinel lherzolite solidus leading to the possibility that $D_{REE}$ may be yet higher (or lower) than predicted. Our aim here is to

determine experimentally trace element partition coefficients under $P$–$T$–$X$–$O_2$ conditions that approximate those during the first degrees (3%) of mantle melting in the spinel stability field.

Robinson et al. [7] found that for fertile lherzolite composition MORB-pyrolite (MPY) the solidus temperature at 1.5 GPa is $1265 \pm 10$°C. As our starting material we have synthesised the glass (#43) shown previously to be in equilibrium with olivine, two pyroxenes and spinel at 1.5 GPa, 1269°C [7], and added to it a variety of trace elements at the ppm level using 1000 ppm AA standard solutions (Table 1). Our choice of elements and doping levels covers a wide range of cation size and charge and, importantly, minimises any isobaric molecular ion interferences that may complicate SIMS analysis (see Appendix A). The starting material was seeded with two small (~100–200 μm) fragments of natural mantle spinel designed to bracket the range of likely equilibrium compositions under these conditions and so ensure spinel saturation.

Experiments were run in an end-loaded piston-cylinder apparatus using graphite-lined Pt capsules with a $CaF_2$ cell and W/Re thermocouple. Prior to encapsulation the starting material was run in a gas-mixing furnace under $CO$–$CO_2$ atmosphere equivalent to 2 log units below FMQ and, after doping, was denitrified at ~300°C and glassed in air in a graphite tub at 1300°C for 1 min. The experiment was run at 1.5 GPa for 47 h. The run temperature, 1255°C, was chosen to be 14°C below the liquidus in order to ensure growth of clinopyroxene large enough for SIMS. Under these conditions the liquid is saturated with clinopyroxene, spinel and plagioclase, rather than the four-phase assemblage observed at 1269°C [7]. This is entirely in keeping with our previous experience of near-solidus melts [7,17], namely that very small changes in experimental pressure ($\pm 50$ MPa) and temperature ($\pm 15$°C) can have a profound effect on the nature of the liquidus phases, but a much lesser effect on their composition. Thus the compositions of melt, spinel and clinopyroxene in our experiment are virtually identical to those in run #48 of Robinson et al. [7] (see below), which is demonstrably in equilibrium with a four-phase spinel lherzolite residuum.

Run products were analysed for major elements by electron microprobe and for trace elements by

Table 1
Chemical compositions of starting materials, run products and calculated partition coefficients

| | Starting materials | | | Run products | | | | | | | | | | Partition coefficients | | | |
|---|---|---|---|---|---|---|---|---|---|---|---|---|---|---|---|---|---|
| | Glass #43 | Seed A DAR-8506-3[c] | Seed B MOZ1[c] | Cpx | s.d. | Plag | s.d. | Glass | s.d. | Spinel microlites | s.d. | Spinel rim | s.d. | Cpx | s.d. | Plag | s.d. |
| n[a] | 15 | 5 | 17 | 13(5) | | 10(2) | | 12(4) | | 5 | | 6 | | | | | |
| $SiO_2$ | 52.89 | 0.04 | 0.02 | 50.24 | 0.49 | 56.04 | 0.26 | 50.17 | 0.47 | 0.38 | 0.16 | 0.14 | 0.02 | 1.001 | 0.0013 | 1.117 | 0.012 |
| $TiO_2$ | 1.07 | 0.06 | 0.08 | 0.76 | 0.09 | 0.04 | 0.05 | 1.15 | 0.04 | 0.24 | 0.03 | 0.22 | 0.02 | | | | |
| $Al_2O_3$ | 21.03 | 51.15 | 60.63 | 10.47 | 0.65 | 26.44 | 0.27 | 20.41 | 0.15 | 65.61 | 1.54 | 66.01 | 1.70 | 0.51 | 0.03 | 1.3 | 0.02 |
| $Cr_2O_3$ | 0.03 | 15.68 | 7.07 | 0.19 | 0.06 | bd | | 0.03 | 0.05 | 2.74 | 1.52 | 2.67 | 0.82 | | | | |
| FeO | 4.74 | 12.29 | 10.96 | 6.70 | 0.33 | 0.34 | 0.19 | 6.06 | 0.22 | 10.36 | 0.48 | 10.47 | 0.33 | 1.10 | 0.07 | 0.06 | 0.03 |
| MnO | bd | 0.13 | 0.10 | 0.02 | 0.02 | bd | | 0.02 | 0.02 | bd | | bd | | | | | |
| NiO | bd | 0.38 | 0.41 | 0.01 | 0.02 | bd | | 0.02 | 0.03 | bd | | 0.05 | 0.04 | | | | |
| MgO | 6.32 | 19.85 | 20.87 | 19.29 | 1.01 | 0.24 | 0.20 | 5.94 | 0.12 | 21.22 | 0.38 | 21.43 | 0.77 | 3.25 | 0.18 | 0.040 | 0.034 |
| CaO | 6.46 | bd | 0.01 | 10.44 | 0.88 | 8.23 | 0.17 | 6.13 | 0.07 | 0.11 | 0.03 | 0.03 | 0.02 | 1.70 | 0.15 | 1.34 | 0.03 |
| $Na_2O$ | 7.49 | 0.01 | bd | 1.39 | 0.13 | 6.63 | 0.20 | 7.29 | 0.20 | 0.03 | 0.02 | bd | | 0.190 | 0.019 | 0.91 | 0.04 |
| Total | 100.00 | 99.59 | 100.15 | 99.51 | | 97.96 | | 97.22 | | 100.69 | | 101.02 | | | | | |
| Mg#[b] | 0.704 | 0.742 | 0.772 | 0.837 | | | | 0.636 | | 0.785 | | 0.785 | | 0.34[d] | | | |
| $X_{An}$ | | | | | | 0.407 | | | | | | | | – | | 1.48[e] | |
| Li | 36 | na | | 8.0 | 0.7 | 4.8 | 0.1 | 31.6 | 0.2 | | | | | 0.254 | 0.022 | 0.151 | 0.002 |
| Sc | 46 | <1.8 | | 150 | 7 | bd | | 46.9 | 0.3 | | | | | 3.20 | 0.15 | bd | |
| Ti | | 581 | | 3866 | 137 | 338 | 27 | 5450 | 18 | | | | | 0.71 | 0.03 | 0.062 | 0.005 |
| V | 20 | 582 | | 160 | 8 | bd | | 32 | 5 | | | | | 5.1 | 0.9 | bd | |
| Ga | 135 | 79 | | 144 | 22 | 83 | 16 | 209 | 20 | | | | | 0.69 | 0.12 | 0.36 | 0.08 |
| Sr | 43 | 1.1 | | 30 | 17 | 598 | 4 | 270 | 2 | | | | | 0.062[f] | 0.004 | 2.21 | 0.02 |
| Y | 90 | <0.4 | | 95 | 4 | 1.4 | 0.4 | 75.1 | 1.0 | | | | | 1.27 | 0.06 | 0.019 | 0.005 |
| Zr | 176 | 8 | | 57 | 5 | 1.2 | 1.0 | 210 | 4 | | | | | 0.27 | 0.03 | 0.006 | 0.005 |
| Nb | 170 | <2 | | 2.3 | 0.8 | 0.8 | 0.7 | 115.5 | 1.0 | | | | | 0.020 | 0.007 | 0.007 | 0.006 |
| La | 86 | na | | 4.4 | 1.0 | 7.4 | 0.4 | 49.2 | 0.9 | | | | | 0.089 | 0.021 | 0.151 | 0.008 |
| Ce | 90 | na | | 12.1 | 1.4 | 8.8 | 1.0 | 75.9 | 0.6 | | | | | 0.160 | 0.018 | 0.117 | 0.014 |
| Nd | 690 | na | | 199 | 9 | 44 | 6 | 547 | 4 | | | | | 0.36 | 0.02 | 0.081 | 0.011 |
| Sm | 780 | na | | 299 | 15 | 24 | 5 | 447 | 5 | | | | | 0.67 | 0.03 | 0.053 | 0.012 |
| Eu | 1475 | na | | 378 | 51 | 1034 | 108 | 994 | 12 | | | | | 0.38 | 0.05 | 1.04 | 0.11 |
| Gd | 350 | na | | 285 | 11 | 13.0 | 1.6 | 289 | 5 | | | | | 0.99 | 0.04 | 0.045 | 0.005 |
| Er | 350 | na | | 406 | 24 | 3.3 | 1.8 | 282 | 6 | | | | | 1.44 | 0.09 | 0.012 | 0.006 |
| Yb | 180 | na | | 119 | 18 | | | 83 | 11 | | | | | 1.43 | 0.29 | | |
| Lu | 180 | na | | 210 | 17 | 1.9 | 1.2 | 142 | 3 | | | | | 1.48 | 0.12 | 0.013 | 0.009 |
| Hf | 30 | <0.9 | | 16.9 | 1.7 | 0.3 | 0.2 | 30.7 | 1.1 | | | | | 0.55 | 0.06 | 0.010 | 0.008 |
| Ta | 50 | <0.5 | | 2.4 | 0.7 | 1.0 | 0.5 | 45 | 2 | | | | | 0.053 | 0.016 | 0.023 | 0.010 |

All major element oxides (incl. $TiO_2$) determined as wt% by electron-microprobe. Trace elements (incl. Ti) determined as ppm by SIMS, except in glass #43 (weighed-in values) and spinel DAR8506-3 (unpublished LA–ICP–MS data); na is not analysed, bd is below detection.
[a] Number of analyses by EMP and (in parentheses) SIMS. [b] Mg# is molar $Mg/(Mg+Fe_{tot})$. [c] Spinel seeds added to #43 glass to make starting material. [d] $K_d$ (Fe/Mg). [e] $K_d$ (Ca/Na). [f] $D_{Sr}$ calculated from two lowest clinopyroxene values due to possibility of plagioclase contamination in others.

SIMS using an ion-microprobe. Full analytical details are given in the Appendix A.

## 3. Results

Run products were ~90% homogeneous glass, ~3% subhedral clinopyroxene, ~7% plagioclase laths ($An_{40.7\pm0.3}$), and trace aluminous spinel (Fig. 1). Phase compositions are reported in Table 1. The glass is an alkali olivine basalt with ~20% normative nepheline. Spinel formed both thin (4 μm) rims on the seed crystals and tiny microlites of similar composition (Table 1) distributed throughout the charge. Clinopyroxene is aluminous sub-calcic augite, with Mg# of 0.84 and ~16 mol% CaTs and ~9 mol% jadeite. The chemistry of stoichiometric analyses of cores and rims is remarkably similar, with $Al_2O_3$ and $Na_2O$ showing the greatest variation of 6 and 10% relative, respectively. The presence of plagioclase at this pressure is simply a consequence of the sub-liquidus temperature of the experiment, and the high Na and Al contents of the liquid [17].

The major element compositions of clinopyroxene and glass (Table 1) are sufficiently close to those at 1.5 GPa, 1269°C [7] to be consistent with formation on the solidus of spinel lherzolite (Fig. 2). The low Ca/Al, Mg# and Cr content, and high Na content of the clinopyroxene place it at the low melt-fraction end of trends produced by partial melting of variously fertile lherzolites (Fig. 2). Similarly the liquid matches the composition of low-degree melts of spinel lherzolite, i.e. low Mg# and Ca/Al, high $Na_2O$ and $SiO_2$ [7–9]. These chemical features are characteristic of the spinel lherzolite solidus and are quite distinct from clinopyroxenes and glasses produced in all other trace element partitioning studies. For example the only other clinopyroxene–melt partition coefficients obtained under similar *P–T* conditions (1.5 GPa, 1265–1275°C [18]) have clinopyroxene and melt compositions inconsistent with low-degree partial melting of the mantle (Fig. 2). As we shall demonstrate, these differences account for the radically different partition coefficients observed in the two sets of experiments.

Trace element chemistry of clinopyroxene, plagioclase and glass is presented in Table 1. All phases
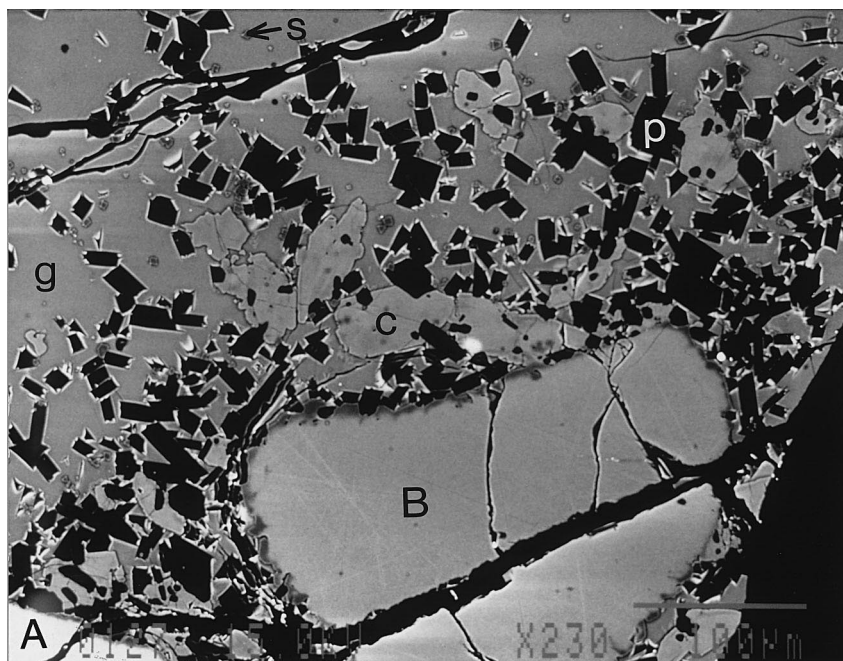


Fig. 1. Back-scattered electron photomicrograph of quenched run products showing plagioclase (*p*), glass (*g*), clinopyroxene (*c*), spinel seeds (*A* and *B*; see Table 1) with thin rims, and spinel microlites (*s*). Scale bar is 100 μm.
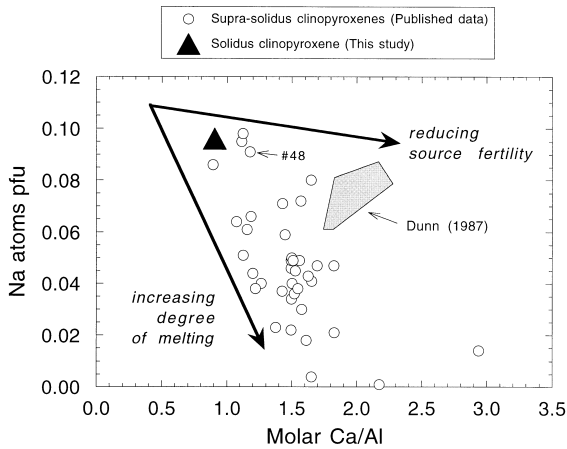
Fig. 2. Compositions of experimental clinopyroxenes (open circles) in equilibrium with melt + olivine + orthopyroxene + spinel at $1.5 \pm 0.1$ GPa [7,20,35–39] in terms of Na atoms per six oxygens versus molar Ca/Al. The labelled arrows denote the effect on clinopyroxene composition of (1) reducing the fertility of the source at constant melt fraction, and (2) increasing the degree of melting for a fixed bulk composition. The composition of our clinopyroxene (large triangle) is similar to that from run #48 of Robinson et al. [7] and therefore consistent with equilibrium with very low-degree partial melts of fertile spinel lherzolite. The stippled field shows the range of clinopyroxenes from the trace element partitioning experiments of Dunn [18]. These are too poor in Na and Al to represent near-solidus compositions.

are homogeneous to within better than $\pm 10\%$ relative for all elements present at concentrations >5 ppm, except those for which interference corrections were made (e.g. Yb, Ga). The unusually large s.d. for Sr in clinopyroxene ($\sim 50\%$ relative; Table 1) may be due to contamination by sub-microscopic plagioclase inclusions: for the purposes of the partition coefficient calculation we used only the two lowest (least contaminated) values obtained.

## 4. Partition coefficients

Partition coefficients for clinopyroxene and plagioclase are given in Table 1 and plotted in Figs. 3 and 4. For clinopyroxene, partition coefficients for REE are higher than those reported in any previous experimental study, including Dunn [18] and Hart and Dunn [15]. The differences are greatest for HREE (Gd, Y, Er, Yb, Lu), which are found to be compatible ($D = 1$). Eu shows a slight nega-

tive anomaly compared to adjacent REE (Fig. 4a). Partition coefficients for the high field strength elements (Ti, Zr, Hf, Nb, Ta) are also high relative to those of Hart and Dunn [15]. Nb is fractionated from Ta with $D_{Nb}/D_{Ta} = 0.38 \pm 0.17$, in keeping with other experimental studies of clinopyroxene [19]. $D_{Na}$ ($0.19 \pm 0.02$) is appreciably lower than the value obtained from the model of Blundy et al. [20], i.e. $0.34 \pm 0.02$, a feature which appears to be characteristic of low-degree mantle melts [7]. For plagioclase all trace elements are incompatible except Sr and Eu, which shows a strong positive anomaly (Fig. 4b).

A good measure of the equilibrium nature of the measured partition coefficients lies in the homogeneity of the mineral and glass phases, and in the systematic behaviour of isovalent cations with ionic radius [21]. At a given $P$ and $T$ equilibrium partition coefficients for isovalent ($n+$) series of cations entering a particular lattice site describe smooth near-parabolic curves when plotted against ionic radius, with maxima corresponding to the size of the lattice site ($r_o$), and a curvature proportional to the effective Young modulus of the site for substitution by $n$-valent cations ($E_{n+}$; [21]). Our clinopyroxene REE partitioning data yield fit parameters $E_{3+}$ and $r_o$ (Fig. 4a) for the large M2 site that are in excellent agreement with those obtained from other partitioning studies [13,21]. Note that disequilibrium growth will produce more open parabolas systematically closer to unity and, therefore, cannot account for $D_{HREE} > 1$.

Several previous experimental studies of basaltic systems have produced $D_{HREE} > 1$ (e.g. [22,23]), and it is well known that HREE partition coefficients are greater than unity in silicic systems [24]. However, this is the first time that HREE partition coefficients have been observed at $P$–$T$–$X$ conditions directly applicable to mantle melting. The compatibility of HREE in our experiment is reflected in the high value for $D_o$ ($1.47 \pm 0.04$; Fig. 4a), the strain-free partition coefficient for a REE with radius $r_o$ [25], which is related to the free energy of fusion of a fictive end member REE pyroxene [13]. The corresponding $D_o$ values for the 1.5 GPa experimental clinopyroxenes of Dunn [18], calculated from $D_{Lu}$ in the fashion described by Wood and Blundy [13], is $0.62 \pm 0.04$ at 1265ºC and $0.62 \pm 0.03$ at 1275ºC. We

Fig. 3. Partition coefficients for clinopyroxene compared to values from Hart and Dunn [15] and Dunn [18]. Elements are ordered along the abscissa with approximate mantle compatibility, after Hofmann [40], increasing to the right. Error bars, for new data only, are 1 s.d.

propose that the high value of our $D_o$ reflects the low value of $D_{Na}$, which in turn reflects the CaTs-rich nature of the clinopyroxene. This can be readily shown by comparison of the equilibrium constants for both sets of data for the relevant partitioning reaction.

Following Wood and Blundy [13] we consider that REE partitioning in Na and Al-rich melts is controlled by the fusion reaction:

$$\underset{\text{pyroxene}}{Na_{0.5}REE_{0.5}\,MgSi_2O_6} = \underset{\text{melt}}{Na_{0.5}REE_{0.5}\,MgSi_2O_6} \quad (1)$$

for which the equilibrium constant, $K_o$, at fixed $P$ and $T$, is given by:

$$K_o = \frac{X_{Mg}^{M1} \cdot \sqrt{D_{Na} \cdot D_o}}{Mg\#_{melt}} \quad (2)$$

where $X_{Mg}^{M1}$ is the mole fraction of Mg on the clinopyroxene M1 site (assuming equipartitioning of Mg and Fe between M1 and M2). Using the data in Table 1 for our clinopyroxene (at 1255°C) we calculate $K_o = 0.62 \pm .07$. The average values for the 1.5 GPa experiments of Dunn [18] are $0.65 \pm .07$ at 1265°C and $0.48 \pm .04$ at 1275°C. The agreement between our value at 1255° and that at 1265°C is well within analytical and experimental error indicating that (a) the differences between our $D_{Lu}$ values and those of Dunn [18] are entirely due to chemical differences (especially $D_{Na}$ and $X_{Mg}^{M1}$) between the two experiments, and (b) the simple activity–composition relationships implicit in Eq. 2 are applicable to Na and Al-rich low-degree partial melts.

In contrast the value of $D_o$ predicted from the alternative fusion reaction of an REE-pyroxene [13], i.e.:

$$\underset{\text{pyroxene}}{REEMgAlSiO_6} = \underset{\text{melt}}{REEMgAlSiO_6} \quad (3)$$

is 0.84, rather less than that observed. This discrepancy suggests that the very simple activity–composition models for $REEMgAlSiO_6$ used by Wood and Blundy [13] do not hold for the Na–Al-rich melt compositions of low-degree mantle melts. In such circumstances Eq. 1 offers a better description of REE partitioning, provided $D_{Na}$ can be independently constrained.

Our high $D_{REE}$ evidently result largely from the low $D_{Na}$ at the spinel lherzolite solidus, which is itself a consequence of the high CaTs content of the experimental clinopyroxene. $Na^+$ has an ionic radius of 1.18 Å [26], which is slightly larger than the M2-site in diopside ($r_o \sim 1.04$ Å [13]). With increasing CaTs content $r_o$ decreases [13,25] making incorporation of Na onto M2 more difficult and so decreasing $D_{Na}$. It is straightforward to estimate the magnitude of this effect from equation 3 of Blundy and Wood [21], assuming that $E_{1+} \approx 1/3E_{3+} \approx 87$ GPa. At a given $P$ and $T$, changing $r_o$ from 1.04 Å to 0.98 Å (Fig. 4a) will reduce $D_{Na}$ by a

Fig. 4. Non-linear weighted least-squares fits (solid curves) to the REE partitioning data for (a) clinopyroxene and (b) plagioclase using the lattice strain model of Blundy and Wood [21]. Ionic radii (Å) in 8-fold co-ordination from Shannon [26]. Eu was not included in the fitting routine. Fit parameters $D_o$, $E_{3+}$ and $r_o$ are given in the boxes, where they are compared to predicted values of $E_{3+}$ and $r_o$ for clinopyroxene [13] and plagioclase [21]. Error bars are 1 s.d.

factor of ∼2, in keeping with our observations. This effect was not accounted for in the Na partitioning model of Blundy et al. [20] because none of the clinopyroxenes studied were sufficiently CaTs-rich to make correction for variation in $r_o$ worthwhile. However, it is now clear that, close to the mantle solidus, clinopyroxenes are sufficiently rich in CaTs to discriminate against Na and so elevate $D_{REE}$. We are presently refining the model of Blundy et al. [20] to take account of crystal–chemical effects on Na partitioning and so provide a means of accurately predicting $D_{Na}$, for inclusion in Eq. 2.

Plagioclase–melt $D_{REE}$ can also be fitted to the Brice equation (Fig. 4b), yielding values of $E_{3+}$ and $r_o$ in good agreement with the values obtained ex-

perimentally in the system diopside–albite–anorthite [21]. These features are again suggestive of trace element equilibrium. There are remarkably few high-pressure plagioclase–melt partition coefficients with which to compare the new data; however, we note that $K_{d,Ca–Na}$ in our experiment (1.47 ± .07) is in reasonable agreement with a model value of 1.67 [27].

## 5. Variation in REE partitioning during mantle melting

The observed relationship between $D_{Na}$ and $D_o$ can be used to constrain, for the first time, the changes in $D_{REE}$ that occur as partial melting progresses. The experiments of Robinson et al. [7] provide values of $D_{Na}$ over the melting interval 0.8–21 wt%. Refitting a subset of the data considered by Wood and Blundy [13], for which $D_{Na}$ is known within 15% relative, gives the following expression for $K_o$ (Eq. 2):

$$RT \ln K_o = 85.667 - 0.0742T + 14.39P - 1.11P^2 \tag{4}$$

where $R$ is the gas constant (0.008314 kJ mol$^{-1}$), $T$ is in K and $P$ is in GPa. This equation yields a value of $K_o$ at 1.5 GPa, 1255ºC of 0.51 in good agreement with our experiment. Combining this expression with the clinopyroxene compositions and values of $D_{Na}$ obtained experimentally [7] enables us to calculate $D_o$ (and hence $D_{REE}$) as a function of melt fraction ($F$; Fig. 5). As temperature, $X_{Mg}^{M1}$ and $D_{Na}$ all increase with increasing $F$ [7], so $D_o$ falls from an initial value of 1.75 at the solidus to 0.41 at $F = 0.25$. The decrease is greatest over the first 5–10% melting, and at $F = 0.25$ the value of $D_o$ approaches that of Hart and Dunn [13], i.e. 0.44 ± 0.01 (Fig. 5).

Our results demonstrate that $D_{REE}$ varies by a factor of 4 over the course of isobaric mantle melting, and that for the first ∼5 wt% of melting the HREE are compatible in clinopyroxene. The situation will be further complicated by the fact that melting is a polybaric process. Since the first melts are generated at higher pressures (and temperatures) on the peridotite solidus, which tends to lower $D_o$ [13,14], so the variation in $D_o$ should be slightly less extreme than in Fig. 5. Nevertheless the potential pitfalls of
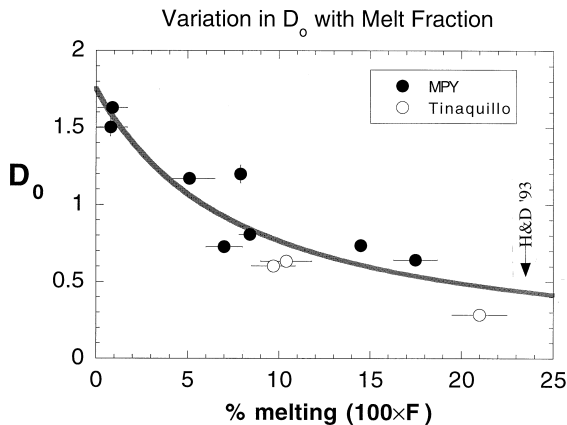
Fig. 5. Variation in the strain-compensated partition coefficient $D_o$ with melt fraction, based on the experimental data of Robinson et al. [7] from MPY and Tinaquillo lherzolite (TQL). Each data point is calculated using the experimental clinopyroxene composition, glass Mg# and $D_{Na}$ and the equilibrium constant from Eq. 4. The melt fractions are relative to fertile mantle composition MPY. Thus for MPY (solid symbols) the melt fractions are those quoted by Robinson et al. [7], while for the more depleted TQL composition we have modified the melt fractions to take account of the fact that TQL is equivalent to MPY after removal of $7.4 \pm 0.2$ wt% partial melt. $D_{REE}$ can be calculated from $D_o$ using the method of Wood and Blundy [13]. Note the substantial decrease in $D_o$ with melt fraction. At high melt fraction $D_o$ approaches the 3 GPa experimental value of Hart and Dunn [15] (*H&D '93*), widely used in modelling. The grey curve is an empirical fit to the data: $D_o = 13.5/(100F + 7.7)$. Error bars are 1 s.d.

modelling mantle melting using constant partition coefficients are self-evident. Results of modelling mantle melting with a full parameterisation that takes account of these effects will be presented elsewhere [14]. In the next section we discuss some more general implications of the new results for current theories of mantle melting beneath ridges.

## 6. Implications for mantle melting

Our new data clearly have implications for those aspects of mantle geochemistry which require knowledge of trace element partitioning behaviour. Obviously results of a single experiment at 1.5 GPa cannot be extrapolated to the entire polybaric process of MORB generation. However, our data pertain to near-solidus melting of spinel lherzolite, wherein the bulk of a MORB liquid is generated, and can

therefore be used to draw some inferences, while recognising that more data on the variation of partition coefficients with *P*, *T* and source composition are required. We will confine ourselves here to a discussion of the REE patterns in MORB glasses and the Lu–Hf and Sm–Nd isotope systematics of MORB. Results of an experimental study of U and Th partitioning using a similar starting composition will be presented elsewhere [28], and we will not discuss U–Th disequilibria studies here. Until we have experimental data on the redistribution of trace elements between clinopyroxene and orthopyroxene during sub-solidus re-equilibration we cannot extrapolate our results on sub-calcic ($\sim$10 wt% CaO), solidus ($>$1250°C) clinopyroxenes, to the patently sub-solidus ($\leq$1150°C), calcic ($>$20 wt% CaO) clinopyroxenes found in abyssal peridotites (e.g. [3]).

As discussed above, incorporating the predicted *P*–*T* dependence of clinopyroxene $D_{REE}$ into models of mantle melting [14] yields quite different results to the conventional constant partition coefficient models. Using the REEMgAlSiO$_6$ model [13] Blundy and Brodie [14] showed that HREE contents of mantle melts from garnet-free spinel lherzolite are buffered to source-normalised concentrations of $\sim$4.9. Our new REE partitioning data are yet higher than those predicted from the REEMgAlSiO$_6$ model, due to the added effects of crystal chemistry close to the mantle solidus (e.g. Fig. 5). Incorporating this effect into the models [14] simply displaces the buffering to slightly lower source-normalised concentrations ($\sim$4.8). In all cases source-normalised HREE patterns of derivative partial melts from garnet-free sources are nearly flat (Dy/Yb $\leq$ 1.06) because clinopyroxene has $D_{Gd}/D_{Lu} = 0.67 \pm 0.06$ (Table 1). In contrast, garnet tends to strongly fractionate Gd from Lu (e.g. $D_{Gd}/D_{Lu} \approx 0.18$ [29]), such that flat chondrite-normalised HREE patterns in melts of garnet-lherzolite can only be produced if the source itself has sub-chondritic middle to heavy REE ratios (i.e. Gd$_N$/Lu$_N \leq 0.7$ [5]). For example, modelling [14] shows that as little as a 15% addition of a 1% melt of garnet lherzolite to the base of the melting column is sufficient to increase source normalised Dy/Yb above 1.10.

A second feature of our new partitioning data is the relative fractionation of Hf and Lu by

clinopyroxene (Fig. 3). MORB have $^{176}Hf/^{177}Hf$ and $^{143}Nd/^{144}Nd$ ratios that are not supported by their low Lu/Hf and Sm/Nd ratios, indicating that parent–daughter pairs were strongly fractionated during mantle melting [4,5]. The isotope systematics demand that the MORB source region is characterised by a critical partitioning parameter [15], CPP = $D_{Sm}/D_{Nd}/D_{Lu}/D_{Hf}$, less than unity. CPP for garnet is ~0.18 [5,29], while the value for clinopyroxene was determined experimentally to be 0.92 [15]. These observations lead to the conclusion that a significant amount of MORB generation must occur within the garnet lherzolite field [4,5]. In contrast, the experimental clinopyroxene produced here has a CPP-value of 0.68, indicating that the partitioning behaviour of CaTs-rich clinopyroxene resembles garnet more closely than previously thought. The clinopyroxene in the Hart and Dunn [15] experiment on alkali basalt at 3 GPa, 1380°C is also aluminous (~14 wt% $Al_2O_3$), but has higher CaO (~16 wt%) and lower Mg# (~0.75) than our clinopyroxene and therefore does not resemble a spinel lherzolite solidus composition. Consequently their $r_o$ is larger (1.02 Å; [21]), which leads to larger $D_{Na}$ (0.75; model $D_{Na}$ = 0.84 [20]) and lower $D_o$ (0.44). The contrasting partitioning behaviour of superficially similar clinopyroxenes emphasises again the care required in selecting partition coefficients for modelling.

The low value of CPP in our experiment greatly reduces (or even eliminates) the necessary contribution to MORB from melts of garnet lherzolite. To illustrate this we contrast Salters' [5] model of spinel–lherzolite melting, using Hart and Dunn's partition coefficients [15], with a model using the mantle mode and melting reactions of Blundy and Brodie [14] and the clinopyroxene partition coefficients in Table 1. Our model assumes perfect aggregation of melts from a columnar melting region, using the non-modal fractional melting equation (4.15) of Rollinson [30]. Use of a more complex model involving a triangular melting region would not materially affect our findings. Significantly, while Salters [5] concluded that almost no MORB could be generated from melting of spinel lherzolite alone, we find that the slope of the δ(Sm/Nd)–δ(Lu/Hf) trend exhibited by several MORB is entirely consistent with such a process (Fig. 6). This is a direct result of the
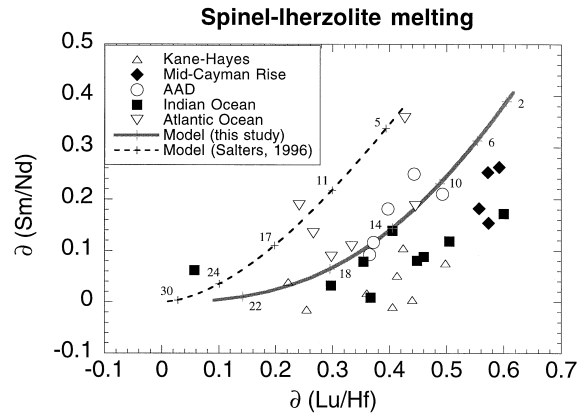


Fig. 6. Plot of source-normalised parent–daughter fractionation factors for Sm–Nd and Lu–Hf, using δ notation [4], for a mean source age of 2 Ga. MORB data are taken from Salters and Hart [4] and Salters [5]. The curves denote modelled variation for melting in the spinel lherzolite field only, assuming aggregated fractional melts from a columnar melting region (see text). The labelled crosses on the curves denote percentage melt fraction. The broken curve uses the data in table 2 of Salters [5], while the solid curve uses the clinopyroxene–melt partition coefficients in Table 1 and the melting reactions and mantle mode of Blundy and Brodie [14]. All other partition coefficients for both curves are taken from Salters' [5] table 2. Note that uncertainty in the age of the source, in the range 1–3 Ga, simply displaces each datum sub-parallel to the bold line.

more 'garnet-like' behaviour of our clinopyroxene. Many MORB remain displaced to the right of the revised model curve in Fig. 6 (i.e. at higher δ(Lu/Hf)), indicating that some other explanation is required for these samples. A sensitivity test on our model establishes that the observed displacement cannot be attributed to uncertainty in the assumed age of the MORB source (2 Ga [5]), nor do changes in melting reaction, mantle mode, or residual porosity, within reasonable limits have any significant effect. Viable alternative possibilities include: (a) the presence of garnet in the source region [4,5]; (b) involvement of crustal material with sub-chondritic Lu/Hf [31]; or (c) further changes in clinopyroxene–melt partitioning at higher pressures within the spinel–lherzolite field. Preliminary calculations, using unpublished garnet partitioning data [29] together with the garnet lherzolite mode and melting reaction of Blundy and Brodie [14], indicate that the data showing the largest deviation from the model (i.e. Kane-Hayes MORB at high δ(Lu/Hf) and δ(Sm/Nd) = 0; Fig. 6)

still require up to 60% of the melt to come from the garnet stability field. We consider this to be implausibly high given the essentially flat chondrite-normalised HREE signature ($Dy_N/Yb_N = 1.06$) of the least evolved basalt glass (Mg# = 0.66) from this area [32]. The available isotopic data for Kane-Hayes MORB [33] render crustal involvement unlikely. We therefore consider that the most likely explanation for the higher $\delta$(Lu/Hf) MORB is that the CPP of clinopyroxene in the spinel stability field continues to decrease as pressure increases beyond 1.5 GPa and solidus clinopyroxenes become still more aluminous [28]. A similar effect may occur for orthopyroxene, which is also known to become increasingly aluminous with pressure. We are presently testing these proposals experimentally in our laboratory.

We conclude that adoption of partition coefficients from experiments carried out under *P–T* conditions that are remote from the lherzolite solidus, and/or on starting materials whose compositions are inappropriate for low-degree mantle melts is inadequate for models of mantle melting. The new clinopyroxene–melt partition coefficients reported here clearly have considerable implications for trace element modelling. However, these partition coefficients apply only to the first 0–5% of melting at 1.5 GPa. As melting proceeds the composition of the residual clinopyroxene and the melt will change, so reducing the partition coefficients towards more conventional values. A further complication arises if reaction between ascending melts and mantle wall-rock (e.g. [34]) modifies trace element behaviour. In any event it is clearly critically important to quantify the variation in solidus clinopyroxene composition with pressure and melt fraction. Then, as our ability to model trace element partitioning as a function of *P–T–X* improves, so we will be able to develop a comprehensive model of trace element behaviour during mantle melting.

## Acknowledgements

## Appendix A. Analytical techniques

Major elements were determined on C-coated polished mounts using a 4-spectrometer JEOL 833 Superprobe at the University of Bristol. Accelerating voltage was 15 kV; beam currents were 15 nA for clinopyroxene and 10 nA for glass. The beam was defocused to ~10 μm for glass analysis to reduce Na loss. Calibrants were albite (Na), diopside (Ca, Si), olivine (Mg), spinel (Al) and oxides.

Trace elements were determined on Au-coated mounts using a Cameca IMS-4f ion-microprobe at the University of Edinburgh. The primary beam was 10.69 keV $O^-$ ions, with a sample current of 2–8 nA corresponding to a spatial resolution of ~20–40 μm. The secondary ion accelerating voltage was 4500 V with an offset of 74–75 V and energy window of $\pm20$ eV to reduce molecular ion transmission. Calibration was performed on NIST glass SRM 610 under similar operating conditions. The following isotopes were measured and ratioed to $^{30}Si$: $^7Li$, $^{42}Ca$, 44, $^{45}Sc$, $^{47}Ti$, $^{51}V$, 67, 68, $^{71}Ga$, $^{88}Sr$, $^{89}Y$, $^{90}Zr$, $^{93}Nb$, $^{139}La$, $^{140}Ce$, $^{143}Nd$, $^{149}Sm$, $^{153}Eu$, $^{157}Gd$, $^{167}Er$, 169, $^{171}Yb$, $^{174}Yb$, $^{175}Lu$, $^{177}Hf$, $^{181}Ta$. Count times were adjusted so as to ensure a statistical precision of better than 10% relative for all isotopes. The following isobaric interferences were monitored and corrected for: $^{29}Si^{16}O$ on $^{45}Sc$; $^{23}Na^{28}Si$ and $^{25}Mg^{26}Mg$ on $^{51}V$; $^{44}Ca^{27}Al$, $^{42}Ca^{29}Si$, $^{43}Ca^{28}Si$, $^{142}Nd^{2+}$ and $^{142}Ce^{2+}$ on $^{71}Ga$; $^{151}Eu^{16}O$ on $^{167}Er$; and GdO on Yb. Average EuO/Eu and GdO/Gd ratios were $0.064\pm0.004$ and $0.14\pm0.03$, respectively, for all phases in agreement with those reported by Hinton [41].

Accuracy of SIMS was assessed from analysis of secondary standards over a four-year period at Edinburgh by JDB. For fused beads of standard basalt glass BIR-1 agreement between SIMS and published analyses [42] is better than $\pm10\%$ relative for REE, Sc, V and Zr. For a clinopyroxene separate from San Carlos (SC8804) agreement between SIMS and unpublished laser-ablation ICP–MS analysis is better than $\pm9\%$ relative for REE (except Yb, $\pm18\%$), Sc, V, Nb and Zr. For analysis of natural materials Hf and Ta are accurate to within $\pm30\%$ relative. Analytical accuracy of our run products is better than this because, by doping our starting materials, we have specifically eliminated isobaric interferences (i.e. $^{161}Dy^{16}O$ on $^{177}Hf$; $^{165}Ho^{16}O$ on $^{181}Ta$) which are unavoidable in natural materials. We have not evaluated the accuracy of our Ga analyses. Systematic underestimates of $16\pm2\%$ relative for Sr, $20\pm4\%$ for Y, ~16% for Li and $14\pm2\%$ for Ti in SIMS analysis of all natural secondary standards at Edinburgh probably reflects differences in secondary ion-yields between Fe-bearing materials and Fe-free SRM 610. Likewise clinopyroxene and glass Ti contents measured by SIMS are 15–20% relative lower than those measured by EMP. The extent of underestimate for these elements is the

same for all phases (glasses, pyroxenes, garnets), demonstrating that in calculation of partition coefficients these effects will cancel out.

# References

[1] T. Shibata, G. Thompson, F.A. Frey, Tholeiitic and alkali basalts from the Mid-Atlantic Ridge at 43°N, Contrib. Mineral. Petrol. 70 (1979) 127–141.

[2] O.P. Tsamerian, A.V. Sobolev, The evidence for extremely low degree of melting under Mid-Atlantic Ridge at 14°N, J. Conf. Abstr. 1 (1) (1996) 628.

[3] K.T.M. Johnson, H.J.B. Dick, N. Shimizu, Melting in the oceanic upper mantle: an ion microprobe study of diopsides in abyssal peridotites, J. Geophys. Res. 95 (1990) 2661–2678.

[4] V.J.M. Salters, S.R. Hart, The hafnium paradox and the role of garnet in the source of mid-ocean ridge basalts, Nature 342 (1989) 420–422.

[5] V.J.M. Salters, The generation of mid-ocean ridge basalts from the Hf and Nd perspective, Earth Planet. Sci. Lett. 141 (1996) 109–123.

[6] B. Bourdon, A. Zindler, T. Elliott, C.H. Langmuir, Constraints on mantle melting at mid-ocean ridges from global $^{238}U$–$^{230}Th$ disequilibrium data, Nature 384 (1996) 231–235.

[7] J.A.C. Robinson, B.J. Wood, J.D. Blundy, The beginning of melting of fertile and depleted peridotite at 1.5 GPa, Earth Planet. Sci. Lett., in press.

[8] M.B. Baker, M.M. Hirschmann, M.S. Ghiorso, E.M. Stolper, Compositions of near-solidus peridotite melts from experiments and thermodynamic calculations, Nature 375 (1995) 308–311.

[9] T.J. Falloon, D.H. Green, H.S.C. O'Neill, W.O. Hibberson, Experimental tests of low degree peridotite partial melt compositions: implications for the nature of anhydrous near-solidus peridotite melts at 1 GPa, Earth Planet. Sci. Lett. 152 (1997) 149–162.

[10] C.C. Lundstrom, H.F. Shaw, F.J. Ryerson, D.L. Phinney, J.B. Gill, Q. Williams, Compositional controls on the partitioning of U, Th, Ba, Pb, Sr and Zr between clinopyroxene and haplobasaltic melts: implications for uranium series disequilibria in basalts, Earth Planet. Sci. Lett. 128 (1994) 407–423.

[11] G.A. Gaetani, T.L. Grove, Partitioning of rare earth elements between clinopyroxene and silicate melt: crystal–chemical controls, Geochim. Cosmochim. Acta 59 (1995) 1951–1962.

[12] J.D. Blundy, J.A. Dalton, Trace-element partitioning between clinopyroxene, silicate melt and carbonate melt in the system diopside–albite–dolomite, in: Seventh Annual V.M. Goldschmidt Conference, LPI Contribution 921, 1997, p. 31.

[13] B.J. Wood, J.D. Blundy, A predictive model for rare earth element partitioning between clinopyroxene and anhydrous silicate melt, Contrib. Mineral. Petrol. 129 (1997) 166–181.

[14] J.D. Blundy, J.A. Brodie, Modelling mantle melting with variable clinopyroxene–melt partition coefficients, Contrib. Mineral. Petrol. (1998) in press.

[15] S.R. Hart, T. Dunn, Experimental cpx/melt partitioning of 24 trace elements, Contrib. Mineral. Petrol. 113 (1993) 1–8.

[16] E.H. Hauri, T.P. Wagner, T.L. Grove, Experimental and natural partitioning of Th, U, Pb and other trace elements between garnet, clinopyroxene and basaltic melts, Chem. Geol. 117 (1994) 149–166.

[17] J.A.C. Robinson, The Experimental Determination of Low-Degree Partial Melts Produced from Peridotite at Upper Mantle Pressures, unpubl. PhD thesis, University of Bristol, 1996, 183 pp.

[18] T. Dunn, Partitioning of Hf, Lu, Ti and Mn between olivine, clinopyroxene and basaltic liquid, Contrib. Mineral. Petrol. 96 (1987) 476–484.

[19] T.H. Green, Significance of Nb/Ta as an indicator of geochemical processes in the crust–mantle system, Chem. Geol. 120 (1995) 347–359.

[20] J.D. Blundy, T.J. Falloon, B.J. Wood, J.A. Dalton, Sodium partitioning between clinopyroxene and silicate melts, J. Geophys. Res. 100 (1995) 15501–15516.

[21] J.D. Blundy, B.J. Wood, Prediction of crystal–melt partition coefficients from elastic moduli, Nature 372 (1994) 452–454.

[22] T.H. Green, N.J. Pearson, Rare earth element partitioning between clinopyroxene and silicate liquid at moderate to high pressure, Contrib. Mineral. Petrol. 91 (1985) 24–36.

[23] P.J. Hack, R.L. Nielsen, A.D. Johnston AD, Experimentally-determined rare-earth element and Y partitioning behaviour between clinopyroxene and basaltic liquids at pressures up to 20 kbar, Chem. Geol. 117 (1994) 89–105.

[24] T.W. Sisson, Pyroxene–high silica rhyolite trace element partition coefficients determined by ion microprobe, Geochim. Cosmochim. Acta 55 (1991) 755–758.

[25] J.D. Blundy, B.J. Wood, A. Davies, Thermodynamics of trace element partitioning between clinopyroxene and melt in the system $CaO$–$MgO$–$Al_2O_3$–$SiO_2$, Geochim. Cosmochim. Acta 60 (1996) 359–364.

[26] R.D. Shannon, Revised effective ionic radii and systematic studies of interatomic distances in halides and chalcogenides, Acta Crystallogr. A32 (1976) 751–767.

[27] T.L. Grove, R.J. Kinzler, W.B. Bryan, Fractionation of mid-ocean ridge basalt (MORB), in: J. Phipps-Morgan, D.K. Blackman, J.M. Sinton (Eds.), Mantle Flow and Melt Generation at Mid-Ocean Ridges, Am. Geophys. Union, Geophys. Monogr. 71 (1992) 281–310.

[28] B.J. Wood, J.D. Blundy, J.A.C. Robinson, Crystal–chemical constraints on partitioning of U-series elements during mantle melting, Geochim. Cosmochim. Acta (1998) submitted.

[29] W. Van Westrenen, J.D. Blundy, B.J. Wood, A.C. Withers, Garnet/melt partitioning of trace elements: theory and experiment, Abstr. Suppl., Terra Nova 9 (1997) 452.

[30] H. Rollinson, Using Geochemical Data: Evaluation, Presentation, Interpretation, Longman, Harlow, 1993, 352 pp.

[31] M. Rehkämper, A.W. Hofmann, Recycled ocean crust and

sediment in Indian Ocean MORB, Earth Planet. Sci. Lett. 147 (1997) 93–106.

[32] J.R. Reynolds, C.H. Langmuir, Petrological systematics of the Mid-Atlantic Ridge south of Kane: implications for ocean crust formation, J. Geophys. Res. 102 (1997) 14915–14946.

[33] L. Dosso, H. Bougault, J.-L. Joron, Geochemical morphology of the North Mid-Atlantic Ridge, 10º–24ºN: trace element–isotope complementarity, Earth Planet. Sci. Lett. 120 (1993) 443–462.

[34] P.B. Keleman, H.J.B. Dick, J.E. Quick, Formation of harzburgite by pervasive melt/rock reaction in the upper mantle, Nature 358 635–641.

[35] E. Takahashi, I. Kushiro, Melting of a dry peridotite at high pressures and basalt magma genesis, Am. Mineral. 68 (1983) 859–879.

[36] D. Elthon, C.M. Scarfe, High pressure phase equilibria of a high magnesia basalt and the genesis of primary oceanic basalts, Am. Mineral. 69 (1984) 1–15.

[37] R.J. Kinzler, T.L. Grove, Primary magmas of mid-ocean ridge basalts 1, Experiments and methods, J. Geophys. Res. 97 (1992) 6885–6906.

[38] H. Hirose, K. Kawamura, A new experimental approach for incremental batch melting of peridotite at 1.5 GPa, Geophys. Res. Lett. 21 (1994) 2139–2142.

[39] R.J. Kinzler, Melting of mantle peridotite at pressures approaching the spinel to garnet transition: application to mid-ocean ridge basalt petrogenesis, J. Geophys. Res. 102 (1997) 853–874.

[40] A.W. Hofmann, Chemical differentiation of the Earth: the relationship between mantle, continental crust, and oceanic crust, Earth Planet. Sci. Lett. 90 (1988) 297–314.

[41] R.W. Hinton, Ion microprobe analysis in geology, in: P.J. Potts, J.F.W. Bowles, S.J.B. Read, M.R. Cave (Eds.), Microprobe Techniques in the Earth Sciences, Chapman and Hall, London, 1995, pp. 235–289.

[42] K. Govindaraju, Compilation of working values and sample description for 383 geostandards, Geostand. Newsl. 18 (1994) 1–158.